2nd URSI AT-RASC, Gran Canaria, 28 May – 1 June 2018

Analysis of Kirchhoff migration and direct sampling method within far-field approximation: from the multi-static to the mono-static configuration

Sangwoo Kang(1), Marc Lambert(1), and Won-Kwang Park(2)
(1) Group of Electrical Engineering, Paris (GeePs),UMR CNRS 8507, CentraleSupélec, Univ. Paris Sud, Université Paris Saclay, UPMC Univ Paris 06, 3 & 11 rue Joliot-Curie 91192, Gif-sur-Yvette, France
(2) Department of Information Security, Cryptology, and Mathematics, Kookmin University, Seoul, 02707, Korea

Abstract

A recently developed direct sampling method (DSM) is studied in the framework of multi- and mono-static configurations within the far-field hypothesis. A full analysis of the behavior of the DSM has not been provided yet in both cases even if, due to a lack of information compared to multi-static data, the mono-static configurations need an adapted analysis. Thanks to the theoretical analysis based on the asymptotic formula for far-field patterns and small obstacles hypothesis, the behavior of DSM is explained and the reason for which it failed in the mono-static configuration is identified. A modified DSM is then proposed and compared to the classical Kirchhoff migration technique (KM) in order to improve the imaging efficiency of the DSM approach. The theoretical results are supported by numerical experiments with synthetic data.

1 Introduction

The two-dimensional inverse scattering problem is an important topic highly related to many issues in modern human life [1].Yet, it is hard to solve because of its inherent non-linearity and ill-posedness. Various non-iterative reconstruction methods have been investigated to overcome those issues, for example, MUltiple SIgnal Classification (MUSIC), linear sampling method (LSM), and Kirchhoff migration (KM), direct sampling method (DSM), etc. Related works can be found in [2–5] and references. Even though good results can be obtained with multi-static data, full analysis of these methods is needed for a proper comparison of their behaviors. However, since the mono-static configuration is of great interest in various applications a deep understanding and development of effective algorithms is still needed. Existing methods have been adapted and applied as MUSIC [6], LSM [7], KM [8], DSM [9], etc.

DSM is a non-iterative technique which has recently been developed to identify the location and shape of the unknown target from either the measured scattered fields or the far-field patterns. Unlike MUSIC and LSM, DSM does not need any additional operation (SVD, orthogonal projection operator, and solving ill-posed linear integral equations, etc.). Recently, the authors have investigated the mathematical structure of the DSM indicator function in the multi-static configuration using near-field data, proposed an improved version, and confirmed its strong relation with the classical KM [10, 11]. Here, the indicator functions of the normalized Kirchhoff migration (NKM) and DSM using asymptotic formula of far-field patterns in the presence of small inhomogeneities is proposed in both multi- and mono-static configurations. The limitation of the classical DSM in the latter configuration is identified and a modified DSM is proposed. The correlation between DSM and NKM for multi- and mono-static data is shown. Some numerical experiments with synthetic data are led to support our theoretical results and the effectiveness of the modified DSM.

The paper is as follows. In § 2, the 2D direct scattering problem and the asymptotic formula of far-field pattern are introduced. The structure analysis of KM for the multi-static and the mono-static configurations are presented in § 3 and the one of DSM in § 4. Numerical results are presented in § 5. Conclusions and perspectives are in § 6.

2 Direct scattering problem and asymptotic formula

The 2D direct scattering problem is sketched (Figure 1) in the presence of a set of small dielectric inhomogeneities denoted as $\tau = \bigcup_m \tau_m$, $m = 1, 2, \cdots, M$, τ_m being a dielectric inhomogeneity represented as $\tau_m = \mathbf{r}_m + \alpha_m \mathbf{B}_m$, where $\mathbf{r}_m$ denotes the location of τ_m, $\mathbf{B}_m$ its simply connected domain with smooth boundary and α_m characterizes its size. In this study, we assume that τ_m are well-separated. For simplicity, we assume that the shape of all τ_m is a ball of radius α_m, i.e., $\mathbf{B}_m = \mathbf{B}$ is unit circle with $|\mathbf{B}| \equiv \pi$.

Here, we assume that every material is non-magnetic ($\mu_m \equiv \mu_0$) and characterized by dielectric permittivity at the angular frequency of operation ω. Let ε_m and ε_0 be the value of electrical permittivity of τ_m and $\mathbb{R}^2$, respectively. Then, we can define the following piecewise constant electrical permittivity at ω such that $\varepsilon(\mathbf{x}) = \varepsilon_m$ for $\mathbf{x} \in \tau_m$ and $\varepsilon(\mathbf{x}) = \varepsilon_0$ for $\mathbb{R}^2 \backslash \overline{\tau}$. With this, we let $k_0 = \omega\sqrt{\varepsilon_0 \mu_0} = 2\pi/\lambda$ be the wavenumber with positive wavelength λ, which satisfies $\alpha_m \ll \lambda/2$ for all $m = 1, 2, \cdots, M$.

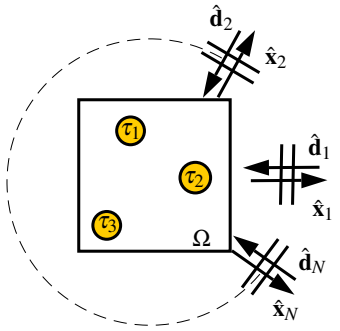

Figure 1. Scattering problem configuration for $M = 3$.

The incident field is a plane-wave, i.e., $u^i(\mathbf{x}) = \mathrm{e}^{\mathrm{i}k_0\hat{\mathbf{d}}\cdot\mathbf{x}}$ with a direction of propagation $\hat{\mathbf{d}} \in \mathbb{S}^1$, where $\mathbb{S}^1$ denotes the two-dimensional unit circle. Let $u(\mathbf{x},\hat{\mathbf{d}}) = u^i(\mathbf{x},\hat{\mathbf{d}}) + u^s(\mathbf{x},\hat{\mathbf{d}})$ be the time-harmonic total field that satisfies the Helmholtz equation with transmission conditions on the boundaries $\partial\tau_m$ and $u^s(\mathbf{x},\hat{\mathbf{d}})$ the scattered field. For uniqueness of solution, $u^s(\mathbf{x},\hat{\mathbf{d}})$ satisfies the Sommerfeld radiation condition.

We denote $u_\infty(\hat{\mathbf{x}},\hat{\mathbf{d}})$ as the far-field pattern of $u^s(\mathbf{x},\hat{\mathbf{d}})$ defined on $\mathbb{S}^1$ that satisfies

$$u^s(\mathbf{x},\hat{\mathbf{d}}) = \frac{\mathrm{e}^{\mathrm{i}k_0\hat{\mathbf{d}}\cdot\mathbf{x}}}{\sqrt{|\mathbf{x}|}}\left[u_\infty(\hat{\mathbf{x}},\hat{\mathbf{d}}) + \mathscr{O}\left(\frac{1}{|\mathbf{x}|}\right)\right] \forall |\mathbf{x}| \to \infty \quad (1)$$

Assuming that τ_m, $m = 1,2,\cdots,M$ are well separated from each other, then for $\hat{\mathbf{x}},\ \hat{\mathbf{d}} \in \mathbb{S}^1$, the far-field pattern $u_\infty(\hat{\mathbf{x}},\hat{\mathbf{d}})$ can be expressed as ([12])

$$\begin{aligned} u_\infty(\hat{\mathbf{x}},\hat{\mathbf{d}}) = &\frac{k_0^2(1+\mathrm{i})}{4\sqrt{k_0\pi}}\sum_{m=1}^{M}\left(\frac{\gamma_m}{\sqrt{\varepsilon_0\mu_0}}\right)|\mathbf{B}_m|\mathrm{e}^{\mathrm{i}k_0(\hat{\mathbf{d}}-\hat{\mathbf{x}})\cdot\mathbf{r}_m} \\ &+ \mathscr{O}(\alpha_m^2) \quad \text{where} \ \ \gamma_m = \alpha_m^2(\varepsilon_m - \varepsilon_0). \end{aligned} \quad (2)$$

In the multi-static configuration all far-field data measured at observation directions $\hat{\mathbf{x}}_n \in \mathbb{S}^1$, $n = 1,2,\cdots,N$ due to impinging plane-waves with propagation directions $\hat{\mathbf{d}}_l \in \mathbb{S}^1$, $l = 1,2,\cdots,L$ are gathered into a Multi-Static Response (MSR) matrix $\mathbb{K} \in \mathbb{C}^{N\times L}$.

$$\mathbb{K} = \begin{bmatrix} u_\infty(\hat{\mathbf{x}}_1,\hat{\mathbf{d}}_1) & u_\infty(\hat{\mathbf{x}}_1,\hat{\mathbf{d}}_2) & \cdots & u_\infty(\hat{\mathbf{x}}_1,\hat{\mathbf{d}}_L) \\ u_\infty(\hat{\mathbf{x}}_2,\hat{\mathbf{d}}_1) & u_\infty(\hat{\mathbf{x}}_2,\hat{\mathbf{d}}_2) & \cdots & u_\infty(\hat{\mathbf{x}}_2,\hat{\mathbf{d}}_L) \\ \vdots & \vdots & \ddots & \vdots \\ u_\infty(\hat{\mathbf{x}}_N,\hat{\mathbf{d}}_1) & u_\infty(\hat{\mathbf{x}}_N,\hat{\mathbf{d}}_2) & \cdots & u_\infty(\hat{\mathbf{x}}_N,\hat{\mathbf{d}}_L) \end{bmatrix}. \quad (3)$$

For the monostatic configuration where $N = L$ and the incident and observation directions coincide, i.e., $-\hat{\mathbf{d}}_n = \hat{\mathbf{x}}_n$, $n = 1,2,\cdots,N$ the mono-static response matrix is written as $\mathbb{K}^{\text{mono}} \in \mathbb{C}^{N\times N}$ as

$$\mathbb{K}^{\text{mono}} = \text{diag}\left[u_\infty(\hat{\mathbf{x}}_1,\hat{\mathbf{d}}_1),\cdots,u_\infty(\hat{\mathbf{x}}_N,\hat{\mathbf{d}}_N)\right], \quad (4)$$

where diag denote the diagonal matrix.

3 Normalized Kirchhoff Migration (NKM)

Let us first introduce the general concepts of NKM in the multi-static measurement configuration. We assume that the total number of incident (L) and observation (M) directions is large enough. For a sampling point $\mathbf{z} \in \Omega$, the indicator function of NKM can be defined as follows:

$$\mathscr{I}_{\text{NKM}}(\mathbf{z}) := \frac{\left|\overline{\mathbf{W}}_1(\mathbf{z})^T\mathbb{K}\overline{\mathbf{W}}_2(\mathbf{z})\right|}{\max\limits_{z\in\Omega}\left|\overline{\mathbf{W}}_1(\mathbf{z})^T\mathbb{K}\overline{\mathbf{W}}_2(\mathbf{z})\right|}. \quad (5)$$

where test vectors $\mathbf{W}_1(\mathbf{z})$ and $\mathbf{W}_2(\mathbf{z})$ are

$$\begin{aligned} \mathbf{W}_1(\mathbf{z}) &= \left[\mathrm{e}^{-\mathrm{i}k_0\hat{\mathbf{x}}_1\cdot\mathbf{z}},\mathrm{e}^{-\mathrm{i}k_0\hat{\mathbf{x}}_2\cdot\mathbf{z}},\cdots,\mathrm{e}^{-\mathrm{i}k_0\hat{\mathbf{x}}_n\cdot\mathbf{z}}\right]^T \ \text{ and} \\ \mathbf{W}_2(\mathbf{z}) &= \left[\mathrm{e}^{\mathrm{i}k_0\hat{\mathbf{d}}_1\cdot\mathbf{z}},\mathrm{e}^{\mathrm{i}k_0\hat{\mathbf{d}}_2\cdot\mathbf{z}},\cdots,\mathrm{e}^{\mathrm{i}k_0\hat{\mathbf{d}}_n\cdot\mathbf{z}}\right]^T. \end{aligned} \quad (6)$$

Thanks to the far-field and small obstacles hypothesis and assuming that the total number of incident (L) and receiving (N) directions is sufficiently large, $\mathscr{I}_{\text{NKM}}(\mathbf{z})$ can then be represented as:

$$\mathscr{I}_{\text{NKM}}(\mathbf{z}) = \frac{|\Psi_1(\mathbf{z})|}{\max\limits_{z\in\Omega}|\Psi_1(\mathbf{z})|}, \Psi_1(\mathbf{z}) = \sum_{m=1}^{M}\gamma_m \mathrm{J}_0(k_0|\mathbf{r}_m - \mathbf{z}|)^2 \quad (7)$$

Let us now focus onto the mathematical structure of the imaging function in the far-field mono-static measurement case. Here also N is assumed to be large enough. $\mathscr{I}^{\text{mono}}_{\text{NKM}}$ can be represented as:

$$\mathscr{I}^{\text{mono}}_{\text{NKM}}(\mathbf{z}) = \frac{|\Psi_3(\mathbf{z})|}{\max\limits_{\mathbf{z}\in\Omega}|\Psi_3|}, \ \ \Psi_3(\mathbf{z}) = \sum_{m=1}^{M}\gamma_m \mathrm{J}_0(2k_0|\mathbf{r}_m - \mathbf{z}|). \quad (8)$$

4 Direct Sampling Method (DSM)

DSM was firstly introduced and applied to 2D inverse scattering problems, refer to [3]. In [13], DSM is applied to the 2D inverse scattering problem when measurement data are far-field patterns. For $\mathbf{z} \in \Omega$, the indicator function of DSM is defined as

$$\mathscr{I}_{\text{DSM}}(\mathbf{z},\hat{\mathbf{d}}) := \frac{|\langle u_\infty(\hat{\mathbf{x}}_n,\hat{\mathbf{d}}),\mathrm{e}^{-\mathrm{i}k_0\hat{\mathbf{x}}_n\cdot\mathbf{z}}\rangle_{L^2(\mathbb{S}^1)}|}{||u_\infty(\hat{\mathbf{x}}_n,\hat{\mathbf{d}})||_{L^2(\mathbb{S}^1)}||\mathrm{e}^{-\mathrm{i}k_0\hat{\mathbf{x}}_n\cdot\mathbf{z}}||_{L^2(\mathbb{S}^1)}}, \quad (9)$$

where

$$\begin{aligned} &\langle a(\hat{\mathbf{x}}_n), b(\hat{\mathbf{x}}_n)\rangle_{L^2(\mathbb{S}^1)} := \sum_{n=1}^{N} a(\hat{\mathbf{x}}_n)\overline{b(\hat{\mathbf{x}}_n)} \approx \int_{\mathbb{S}^1} a(\hat{\mathbf{x}})\overline{b(\hat{\mathbf{x}})}\mathrm{d}\hat{\mathbf{x}} \\ &\text{and} \quad \|a(\hat{\mathbf{x}}_n)\|^2_{L^2(\mathbb{S}^1)} := \langle a(\hat{\mathbf{x}}_n), a(\hat{\mathbf{x}}_n)\rangle_{L^2(\mathbb{S}^1)}. \end{aligned} \quad (10)$$

For multiple impinging directions, the indicator function $\mathscr{I}_{\text{DSM}}(\mathbf{z})$ is defined by

$$\mathscr{I}_{\text{DSM}}(\mathbf{z}) := \max\left\{\mathscr{I}_{\text{DSM}}(\mathbf{z},\hat{\mathbf{d}}_l),\ l = 1,2,\cdots,L\,;\ \mathbf{z}\in\Omega\right\}, \quad (11)$$

where $\mathscr{I}_{\text{DSM}}(\mathbf{z},\hat{\mathbf{d}}_l)$ is the indicator function for the direction of incident field $\hat{\mathbf{d}}_l$, as defined in (9). Within the same

framework as for (7) we can state that, for a fixed incident direction of propagation $\hat{\mathbf{d}}$, $\mathscr{I}_{\mathrm{DSM}}(\mathbf{z})$ can be represented as:

$$\mathscr{I}_{\mathrm{DSM}}(\mathbf{z},\hat{\mathbf{d}}) = \frac{|\Psi_2(\mathbf{z})|}{\max\limits_{z\in\Omega}|\Psi_2(\mathbf{z})|}, \quad \Psi_2(\mathbf{z}) = \sum_{m=1}^{M} \gamma_m \mathrm{J}_0(k_0|\mathbf{r}_m - \mathbf{z}|) \tag{12}$$

For the multiply impinging direction case, it is easy to see that, for $l = 1,2,\ldots,L$,

$$\mathscr{I}_{\mathrm{DSM}}(\mathbf{z}) \propto \max\left\{ \left| \sum_{m=1}^{M} \gamma_m |\mathbf{B}_m| \mathrm{e}^{\mathrm{i}k_0 \hat{\mathbf{d}}_l \mathbf{r}_m} \mathrm{J}_0(k_0|\mathbf{z}-\mathbf{r}_m|) \right| \right\}. \tag{13}$$

According to [9], the indicator function of DSM with mono-static data can be introduced as follows:

$$\mathscr{I}^{\mathrm{mono}}_{\mathrm{DSM}}(\mathbf{z}) := \frac{|\langle u_\infty(\hat{\mathbf{x}}_n,\hat{\mathbf{d}}_n), \mathrm{e}^{-\mathrm{i}k_0\hat{\mathbf{x}}_n\cdot\mathbf{z}}\rangle_{L^2(\mathbb{S}^1)}|}{\max\limits_{\mathbf{z}\in\Omega} ||u_\infty(\hat{\mathbf{x}}_n,\hat{\mathbf{d}}_n)||_{L^2(\mathbb{S}^1)} ||\mathrm{e}^{-\mathrm{i}k_0\hat{\mathbf{x}}_n\cdot\mathbf{z}}||_{L^2(\mathbb{S}^1)}} \tag{14}$$

which can then represented as:

$$\mathscr{I}^{\mathrm{mono}}_{\mathrm{DSM}}(\mathbf{z}) = \frac{|\Psi_4|}{\max\limits_{\mathbf{z}\in\Omega}|\Psi_4|}, \quad \Psi_4(\mathbf{z}) = \sum_{m=1}^{M} \gamma_m |\mathbf{B}_m| \mathrm{J}_0(k_0|2\mathbf{r}_m - \mathbf{z}|). \tag{15}$$

Eq (15) shows that DSM is proportional to $|\mathrm{J}_0(k_0|2\mathbf{r}_m - \mathbf{z}|)|$ and has scaling coefficient which has to be taken into account in the mono-static configuration, i.e, instead of true locations $\mathbf{r}_m$, shifted locations $2\mathbf{r}_m$ are identified via the map of $\mathscr{I}_{\mathrm{DSM}}(\mathbf{z})$. In order to overcome this scaling problem, a modified DSM (MDSM) indicator function is proposed as

$$\mathscr{I}^{\mathrm{mono}}_{\mathrm{MDSM}}(\mathbf{z}) := \frac{|\langle u_\infty(\hat{\mathbf{x}}_n,\hat{\mathbf{d}}_n), \mathrm{e}^{-2\mathrm{i}k_0\hat{\mathbf{x}}_n\cdot\mathbf{z}}\rangle_{L^2(\mathbb{S}^1)}|}{\max\limits_{\mathbf{z}\in\Omega} ||u_\infty(\hat{\mathbf{x}}_n,\hat{\mathbf{d}}_n)||_{L^2(\mathbb{S}^1)} ||\mathrm{e}^{-2\mathrm{i}k_0\hat{\mathbf{x}}_n\cdot\mathbf{z}}||_{L^2(\mathbb{S}^1)}}. \tag{16}$$

5 Numerical experiments

Numerical experiments are provided to support our theoretical results. We consider a fixed frequency $f = c_0/\lambda$ where $c_0 = 1/\sqrt{\varepsilon_0\mu_0}$ is the speed of light and λ the wavenumber $\lambda = 0.4\,\mathrm{m}$. The total number of incident and observation directions is set to $N = L = 36$ evenly distributed on the unit circle. The region of interest (ROI) Ω is a square of side length 4λ uniformly discretized with $N_x \times N_y$ pixels with $N_x = N_y = 50$.

The far-field patterns $u_\infty(\hat{\mathbf{x}}_n,\hat{\mathbf{d}}_n)$ are generated by FEKO (EM simulation software) for Examples 1 and 2. A 20 dB white Gaussian random noise is added.

Example 1 (small disks) First, we consider small dielectric disks τ_m, $m = 1,2,3$. The locations $\mathbf{r}_m$ of τ_m are selected as $\mathbf{r}_1 = (0.75\lambda, -0.75\lambda)$, $\mathbf{r}_2 = (-\lambda, -0.5\lambda)$, and

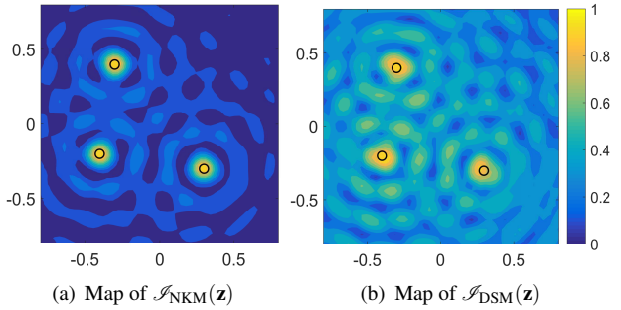

(a) Map of $\mathscr{I}_{\mathrm{NKM}}(\mathbf{z})$ (b) Map of $\mathscr{I}_{\mathrm{DSM}}(\mathbf{z})$

Figure 2. (Example 1) Multi-static configuration.

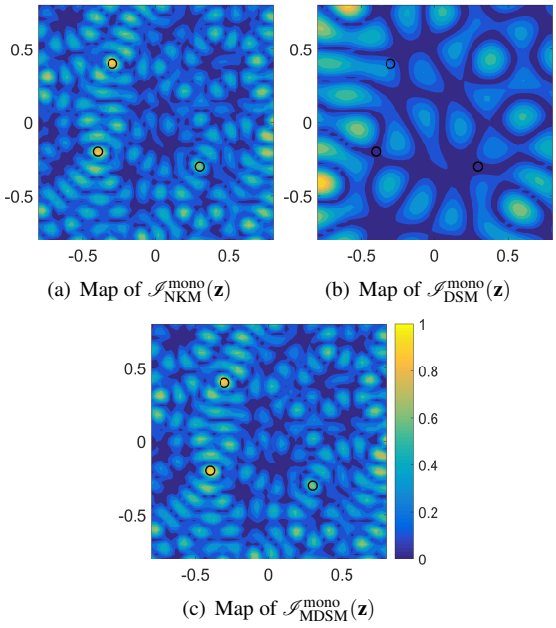

(a) Map of $\mathscr{I}^{\mathrm{mono}}_{\mathrm{NKM}}(\mathbf{z})$ (b) Map of $\mathscr{I}^{\mathrm{mono}}_{\mathrm{DSM}}(\mathbf{z})$

(c) Map of $\mathscr{I}^{\mathrm{mono}}_{\mathrm{MDSM}}(\mathbf{z})$

Figure 3. (Example 1) Mono-static configuration.

$\mathbf{r}_3 = (-0.75\lambda, \lambda)$. In this example, we consider the identification of τ_m with constant radius and permittivity set at $\alpha_m \equiv 0.075\lambda$ and $\varepsilon_m \equiv 5\varepsilon_0$, respectively. According to Figure 2, we can identify the locations of τ_m via the maps $\mathscr{I}_{\mathrm{NKM}}(\mathbf{z})$ and $\mathscr{I}_{\mathrm{DSM}}(\mathbf{z})$ in the multi-static configuration (Figure 2). As expected $\mathscr{I}_{\mathrm{NKM}}(\mathbf{z})$ performed better than $\mathscr{I}_{\mathrm{DSM}}(\mathbf{z})$. In the mono-static configuration (Figure 3) the localization of τ_m is identified via the $\mathscr{I}_{\mathrm{NKM}}(\mathbf{z})$ and $\mathscr{I}_{\mathrm{MDSM}}(\mathbf{z})$ but not via $\mathscr{I}_{\mathrm{DSM}}(\mathbf{z})$ if the scaling problem is not taken into account. Using MDSM solves the problem and leads to a similar behavior as the one of NKM.

Example 2 (large disk) In order to verify that our proposal still works properly when the small obstacle hypothesis is no longer verified, we are considering the case of a single large circular τ located at $\mathbf{r} = (-0.75\lambda, -0.75\lambda)$ with radius $\alpha \equiv 1\lambda = 0.4\,\mathrm{m}$ and permittivity $\varepsilon = 5\varepsilon_0$. From Figure 4, the location and shape of τ_m can be identified via the maps $\mathscr{I}_{\mathrm{NKM}}(\mathbf{z})$ and $\mathscr{I}_{\mathrm{DSM}}(\mathbf{z})$ in the multi-static configuration (Figure 4). In the monostatic one (Figure 5) only the center of τ is identified by both $\mathscr{I}^{\mathrm{mono}}_{\mathrm{NKM}}(\mathbf{z})$ and $\mathscr{I}^{\mathrm{mono}}_{\mathrm{MDSM}}(\mathbf{z})$ whereas the scaling problem still occurred in $\mathscr{I}^{\mathrm{mono}}_{\mathrm{DSM}}(\mathbf{z})$.

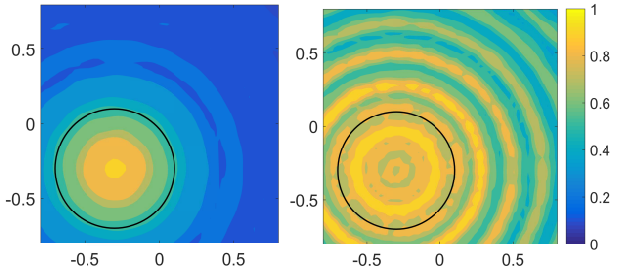

(a) Map of $\mathscr{I}_{\mathrm{NKM}}(\mathbf{z})$ (b) Map of $\mathscr{I}_{\mathrm{DSM}}(\mathbf{z})$

Figure 4. (Example 2) Multi-static configuration.

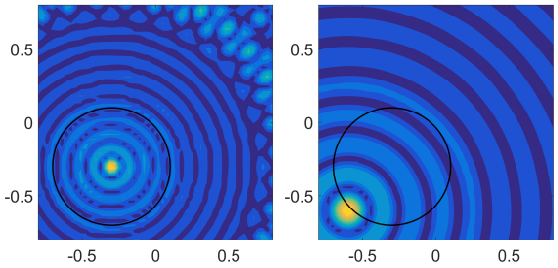

(a) Map of $\mathscr{I}^{\mathrm{mono}}_{\mathrm{NKM}}(\mathbf{z})$ (b) Map of $\mathscr{I}^{\mathrm{mono}}_{\mathrm{DSM}}(\mathbf{z})$

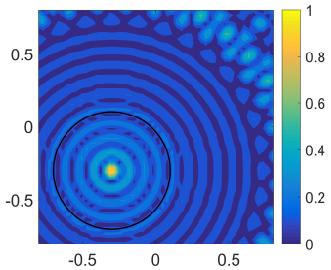

(c) Map of $\mathscr{I}^{\mathrm{mono}}_{\mathrm{MDSM}}(\mathbf{z})$

Figure 5. (Example 2) Mono-static configuration.

6 Conclusion

A mathematical formulation of the NKM and DSM indicator functions in both multi- and mono-static data configurations is proposed in the framework of the asymptotic formula of far-field pattern and the small obstacles hypothesis. Based on such an analysis the limitation of traditional DSM in the mono-static configuration is understood and MDSM is proposed to overcome this limitation. MDSM shows the same efficiency than NKM. Numerical experiments are provided to support our theoretical results.Analysis of NKM and MDSM in multi- and mono-static data for line source is a forthcoming subject as well as the 3D case.

Acknowledgement

The author would like to acknowledge Dominique Lesselier for its comments. W.-K. Park was supported by the Basic Science Research Program of the National Research Foundation of Korea (NRF) funded by the Ministry of Education (No. NRF-2017R1D1A1A09000547).

References

[1] H. Ammari, *An Introduction to Mathematics of Emerging Biomedical Imaging*, ser. Mathematics and Applications Series. Berlin: Springer, 2008, vol. 62.

[2] H. Ammari, J. Garnier, H. Kang, W.-K. Park, and K. Sølna, "Imaging schemes for perfectly conducting cracks," *SIAM J. Appl. Mathi*, vol. 71, no. 1, pp. 68–91, 2011.

[3] K. Ito, B. Jin, and J. Zou, "A direct sampling method to an inverse medium scattering problem," *Inverse Prob.*, vol. 28, no. 2, p. 025003, 2012.

[4] A. Kirsch and S. Ritter, "A linear sampling method for inverse scattering from an open arc," *Inverse Prob.*, vol. 16, no. 1, p. 89, 2000.

[5] W.-K. Park, "Asymptotic properties of MUSIC-type imaging in two-dimensional inverse scattering from thin electromagnetic inclusions," *SIAM J. Appl. Math.*, vol. 75, pp. 209–228, 2015.

[6] J. W. Odendaal, E. Barnard, and C. W. I. Pistorius, "Two-dimensional superresolution radar imaging using the MUSIC algorithm," *IEEE Trans. Antennas Propagat.*, vol. 42, no. 10, pp. 1386–1391, 1994.

[7] I. Catapano, F. Soldovieri, and L. Crocco, "2D GPR imaging via linear sampling method: A performance assessment tool," in *6th International Workshop on Advanced Ground Penetrating Radar (IWAGPR)*. IEEE, 2011, pp. 1–4.

[8] X. Liu, M. Serhir, and M. Lambert, "Detectability of underground electrical cables junction with a ground penetrating radar: electromagnetic simulation and experimental measurements," *Constr. Build. Mater.*, vol. 158, pp. 1099–1110, 2018.

[9] H. O. Bektas and O. Ozdemir, "Direct sampling method for monostatic radar imaging," in *URSI International Symposium on Electromagnetic Theory (EMTS)*. IEEE, 2016, pp. 152–154.

[10] S. Kang, M. Lambert, and W.-K. Park, "Multi-frequency direct sampling method in inverse scattering problem," *J. Phys: Conf. Ser.*, vol. 904, no. 1, p. 012018, 2017.

[11] S. Kang, M. Lambert, and W.-K. Park, "Direct sampling method for imaging small dielectric inhomogeneities: analysis and improvement," *ArXiv e-prints*, p. 1801.05993, Jan. 2018.

[12] H. Ammari and H. Kang, *Reconstruction of Small Inhomogeneities from Boundary Measurements*, ser. Lecture Notes in Mathematics. Berlin: Springer-Verlag, 2004, vol. 1846.

[13] J. Li and Z. Zou, "A direct sampling method for inverse scattering using far-field data," *Inverse Probl. Imag.*, vol. 7, no. 3, pp. 757–775, 2013.